Eur. Phys. J. D **44**, 65–72 (2007)
DOI: 10.1140/epjd/e2007-00156-y

THE EUROPEAN PHYSICAL JOURNAL D

Quenching of molecular ions by He buffer loading at ultralow energies: rotational cooling of $OH^+(^3\Sigma^-)$ from quantum calculations

L. González-Sánchez, E. Bodo, and F.A. Gianturco[a]

Department of Chemistry and CNISM, University of Rome La Sapienza, Piazzale A. Moro 5, 00185 Rome, Italy

Received 18 January 2007 / Received in final form 26 March 2007
Published online 11 May 2007 –

Abstract. An ab initio computed potential energy surface is employed to evaluate the interaction of the $OH^+(^3\Sigma^-)$ molecule with $^4He(^1S)$ atom and an analytic fitting of the raw points is directly employed in quantum scattering calculations at ultralow collision energies. The Hund's case (b) chosen to handle the spin-rotation coupling allows to extract from the numerous inelastic cross sections the relative importance of pure "spin flip" vis-à-vis rotational cooling cross sections. The final rates of all the above processes as a function of the initial $|N\rangle$ state are analysed in detail and possible propensity rules are discussed.

PACS. 34.50.Bw Energy loss and stopping power – 34.50.-s Scattering of atoms and molecules – 34.50.Pi State-to-state scattering analyses

1 Introduction

In recent years the study of translationally cold (in the millikelvin regime) molecular ions embedded in coulomb crystals has provided a range of information on the special conditions created by their environment: from the high-precision measurements of their ro-vibrational spectral features to the chance of carrying out state-selective studies of chemical reactions. In particular, diatomic molecular hydrides like ArH^+ and ArD^+ have proven to be very useful for testing the time dependence of fundamental quantities like the particle mass ratios [1] or for providing model systems for implementing internal state manipulation schemes [2]. In this last instance, molecules with relatively simple hyperfine structure are more favourable in order to minimize the number of laser sources needed to carry out internal cooling procedures.

Furthermore, because of their relative abundance in the interstellar clouds (ISC), the chemistry of hydrogen-containing molecular ions is of direct interest to astrochemical investigation [3,4] since chemical reactions between state-prepared molecular ions and (possibly state-prepared) neutral molecules are usually exothermic when excited vibrational levels are involved and therefore could be profitably studied inside Coulomb crystals. Under strong cooling conditions, e.g. down to the 50 mK regions, the ions can undergo a phase transition to an ordered state (the Coulomb crystal) characterized by well-defined sites being occupied by the molecular ions [5,6] with typical interparticle distances of a few tens of micrometer.

A powerful method for cooling molecular ions, or for possibly selecting specific rotational states to be populated at ultralow energies, is therefore the use of the sympathetic cooling by collision. One could hence envisage possible interaction with additional neutral partners and thus analyse the selective efficiency of producing the molecular ions in specific ro-vibrational states [7]. In the present computational study we have chosen to study the collisional cooling of the molecular ionic hydride $OH^+(^3\Sigma^-)$ interacting with a simple neutral partner, the $^4He(^1S)$ atom. We have carried out full quantum calculations of the rotationally elastic and inelastic cross sections down to the μK regime in order to see if the corresponding relaxation rates reveal the existence of some propensity rules which apply during the scattering process and which would allow us to forecast specific optimal conditions under which the molecular ions could be more efficiently prepared. The subject of ultralow energy collisions with open-shell diatomics has been discussed in earlier theoretical and computational work, like the O_2 system in collision with He [8,9], while the relative conservation of spin states during rotational relaxation has also been recently analysed [10,11]. More general reviews on the same subject could be found in references [12,13].

The remaining of this paper is organized as follows: the next section outlines the features of the relevant potential energy surface between the molecular ion in its ground electronic state and the neutral helium atom. It also summarizes the rotational structure of OH^+ and the coupling

[a] e-mail: fa.gianturco@caspur.it

of spin-rotational angular momenta employed during the quantum dynamics.

Section 3 reports our present results for both cross sections and relaxation rates while Section 4 summarizes our conclusions.

2 Interaction and dynamics

2.1 The potential energy surface (PES)

The interaction between the hydroxyl cation and the neutral ^{4}He atom has been computed by us earlier and described there in great detail [14]: we therefore provide here only an outline of its main features. The calculations were carried out at the post-Hartree-Fock level by using the MP4 formalism, within a basis set expansion of the aug-cc-pVQZ quality that included BSSE corrections via the familiar counterpoise method [15]. The computed orientations of the helium projectile with respect to the molecular target treated as a rigid rotor (i.e. at its fixed equilibrium bond distance of r_{eq} = 1.0279 Å), were those given in Jacobi coordinates by 12 different values of the relative angle ϑ, over a radial range from 2.0 to 4.35 Å with a spacing ΔR = 0.11 Å. The above 24 values per chosen ϑ were further extended to 10.0 Å with ΔR = 1.0 Å (and for a subset of 5 angular values) for a total of about 320 points.

The whole PES was then represented by using the two-center expansion approach employed in our earlier work [16], whereby we write the overall interaction as

$$V(R,\vartheta|r_{eq}) = V_{sr}(R_A,R_B,\vartheta_A,\vartheta_B) + V_{lr}(R,\vartheta) \qquad (1)$$

where

$$V_{sr} = V_{sr}^{(A)}(R_A,\vartheta_A) + V_{sr}^{(B)}(R_B,\vartheta_B) \qquad (2)$$

and

$$V_{lr} = \frac{c_4 f_4(\beta R)}{R^4} + \frac{c_5 f_5(\beta R)}{R^5}\cos\vartheta. \qquad (3)$$

The two terms on the r.h.s. of equation (2) are given by a set of parameters for the radial coefficients times Legendre polynomials describing the ϑ-dependence. Their actual form was given before [14–16] and all the parameters can be obtained on request from the authors. The (A, B) labels identify the O and H atoms in the target and the angles are those formed between the molecular axis and the distances of the helium partner from each atom, the latter being obviously the $(R_A,\ R_B)$ vectors. The parameter β scales the distance in order to connect (sr) and (lr) regions, the latter being given now by the molecular-centered Jacobi coordinates [14–16]. It ensures that the overall interaction behaves asymptotically as the leading polarization term

$$V_\infty^\alpha(R) \sim \frac{\alpha_0}{2R^4} \qquad (4)$$

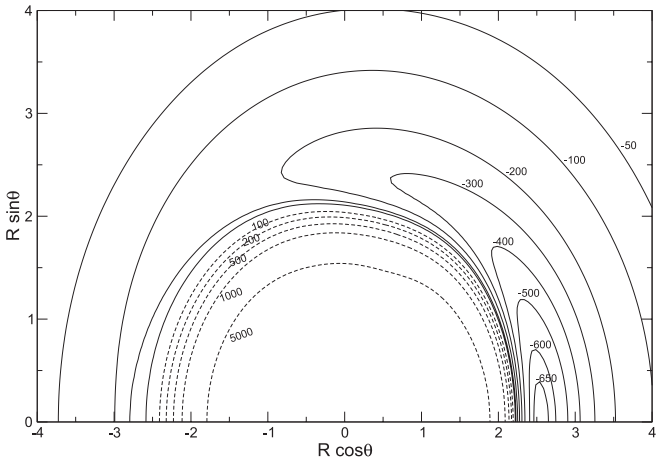

Fig. 1. Pictorial view of the OH^+–He interaction in the short-range region, given by the energy isolines (in cm^{-1}) as a function of $R\cos\vartheta$ and $R\sin\vartheta$ coordinates. The zero locates the molecular center-of-mass close to the oxygen atom. The H atom is positioned along the positive branch of the axis.

where α_0 is the He atom dipole polarizability (1.41 a_0^3). We have also included the dipole-polarization term

$$V_\infty^{\alpha\mu}(R) \sim \frac{2\alpha\mu}{R^5}\cos\vartheta \qquad (5)$$

where the induced dipole comes from the fitting of the PES points and was found to be in good accord with the direct ab initio value quoted in [14–16].

A pictorial view of the surface as a map of isoenergy lines is reported by Figure 1: we clearly see that the potential exhibits a well marked attractive well on the hydrogen side, with a minimum located at about -650 cm^{-1}, and an extension of the attractive region nearly all around the molecular target. This feature therefore surmises a strong anisotropy of the relative orientation between the target molecule and the impinging projectile, a property which we shall see to have direct consequences on the relative efficiency of the rotational quenching of the cation by collision with ^{4}He.

2.2 Rotational structure of the $OH^+(^3\Sigma^-)$

In the $OH^+(^3\Sigma^-)$ state, we have three levels for each total angular momentum $\geq$1: the rotational levels are in fact split by spin-spin and spin-rotation coupling effects. In the pure Hund's case (b) the electronic spin momentum $\mathbf{S}$ couples with the nuclear rotational angular momentum $\mathbf{N}$ ($\mathbf{N} = \mathbf{R}$ for a Σ state) to form the total angular momentum $\mathbf{j}$, given by

$$\mathbf{j} = \mathbf{N} + \mathbf{S}. \qquad (6)$$

Hence, in this coupling scheme, each j level (with $j \geq 1$) is split into three sublevels F_1, F_2, and F_3, and the corresponding rotational wave functions can be written as

$$\begin{aligned} |F_1 jm\rangle &= |N = j-1, Sjm\rangle\,; \\ |F_2 jm\rangle &= |N = j, Sjm\rangle\,; \\ |F_3 jm\rangle &= |N = j+1, Sjm\rangle \end{aligned} \qquad (7)$$

where m is the projection of the **j** along the space-fixed z-axis.

The rotational levels of the molecule may be labeled not only by the above quantum numbers defined in the Hund's case (b) but also by their parity index ε. The levels in molecules of odd multiplicity with parity index equal to 1 are labeled **e**, and those with parity index equal to -1 are labeled **f** [17,18]. However, we shall omit this index in the following discussion since we shall not be using it in our analysis.

For a given N value, the energies of the three levels in equation (7) are given by [19]

$$\begin{aligned} E_{j=N+1} &= BN(N+1) - DN^2(N+1)^2 \\ &\quad - \frac{2\lambda N}{3(2N+3)} + \gamma N \\ E_{j=N} &= BN(N+1) - DN^2(N+1)^2 + \frac{2\lambda}{3} - \gamma \\ E_{j=N-1} &= BN(N+1) - DN^2(N+1)^2 \\ &\quad - \frac{2\lambda(N+1)}{3(2N-1)} - \gamma(N+1) \end{aligned} \tag{8}$$

where B is the rotational constant, and the other constants describe: D the centrifugal distortion, λ the spin-spin interaction, and γ the spin-rotation interaction. The rotational energy levels of the OH^+ molecule were computed using the experimental constants provided by Brown [17] and the energies of some of the lower fine-structure levels are given by Figure 2.

We clearly see in that figure that the $\Delta N \neq 0$ transitions involve much larger energy values than those which cause changes in the spin quantum number **S** that is responsible for the separations between **j** states. Thus, one can say that rotational quenching transitions have much larger energy gaps than those which simply cause spin-flipping processes within each N-labelled manifold.

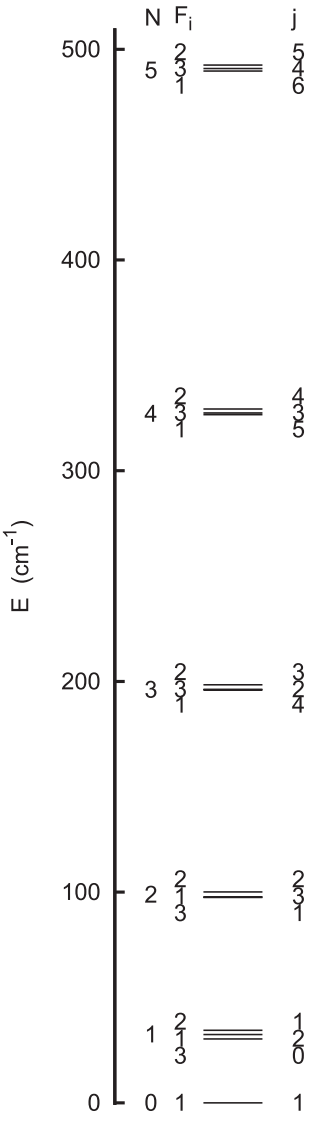

Fig. 2. Rotational levels of the cationic target (all the values in cm^{-1}). The labeling of the levels gives, on the left, the N and F_i quantum numbers while on the right we report the total angular momentum j.

2.3 Scattering calculations

The collision of a molecule in a particular $|F_i jm\rangle$ state with a structureless target is treated by expanding the overall wavefunction in terms of eigenfunctions of the total scattering angular momentum J, namely [21,22] by writing

$$|F_i jLJM\rangle = \sum_{MM_L} \langle jmLM_L|JM\rangle \, |LM_L\rangle \, |F_i jm\rangle \tag{9}$$

here $\langle \cdots | \cdot\cdot \rangle | \cdot\cdot \rangle$ is a Clebsch-Gordan coefficient, M is the projection of J along the space-fixed z-axis, L is the relative orbital angular momentum quantum number, M_L is the projection along z, and $|LM_L\rangle$ is the wave function for the angular motion of the structureless particle. The index F_i refers to the labelling of the spin levels ($i = 1, 2, 3$) reported in equation (7). The target rotational wave functions of equation (9) may also be expressed in a general form

$$|F_i jm\rangle = \sum_{N=j-1}^{N=j+1} c^j_{NF_i} \, |NSjm\rangle. \tag{10}$$

Hence, by solving coupled channel equations we obtain the transition matrix elements and the related cross sections between fine-structure levels. In particular, the potential matrix elements between states $|F_i jLJM\rangle$ and $|F'_i j'L'JM\rangle$ at a fixed total angular momentum J are given by

$$\begin{aligned} &\langle F'_i j'L'JM| \, V \, |F_i jLJM\rangle = \\ &\qquad \sum_{NN'} c^{j'}_{N'F'_i} c^j_{NF_i} \, \langle N'S'j'L'JM| \, V \, |NSjLJM\rangle \end{aligned} \tag{11}$$

where the matrix elements of V between pure Hund's case (b) basis functions are given by $\langle N'S'j'L'JM| \, V \, |NSjLJM\rangle$ [23].

We have carried out calculations by solving the relevant coupled-channel equation for all the initial states from $N = 1$ to $N = 8$. Several closed channels were included in order to obtain convergence of the collisional cross sections: the range of integration was extended out to 50 000 a_0 maximum and at least ten closed channels were included in each expansion (10). The final cross sections

Table 1. Rotational energies of the OH^+ levels considered in this study.

Level	N	j	F_i	Energy (cm^{-1})
1	0	1	F_1	0.00
2	1	0	F_3	30.28
3	1	2	F_1	32.40
4	1	1	F_2	34.42
5	2	1	F_3	97.49
6	2	3	F_1	97.76
7	2	2	F_2	100.05
8	3	4	F_1	195.87
9	3	2	F_3	196.26
10	3	3	F_2	198.38
11	4	5	F_1	326.57
12	4	3	F_3	327.43
13	4	4	F_2	329.27
14	5	6	F_1	489.65
15	5	4	F_3	490.91
16	5	5	F_2	492.54
17	6	7	F_1	684.90
18	6	5	F_3	686.53
19	6	6	F_2	687.96
20	7	8	F_1	912.02
21	7	6	F_3	914.00
22	7	7	F_2	915.25
23	8	9	F_1	1170.69
24	8	7	F_3	1173.01
25	8	8	F_2	1174.08
26	9	10	F_1	1460.55
27	9	8	F_3	1463.19
28	9	9	F_2	1464.10

are expected to be numerically converged within 0.1% significant figures. The integrator which was employed in the one developed earlier in our group [24,25] and modified to include the additional angular momentum coupling terms afforded by the expansion procedure outlined above. Typically, each of our calculations included a total of about 600 coupled channels in the ultralow energy regions which we extended down to 10^{-6} cm^{-1}.

An indication of the level spacings which exist in the OH^+ cation within the spin-rotational coupling scheme outlined above can be obtained from the list of the first nine rotational states and of all their components reported by Table 1.

3 Collisional observables

3.1 Elastic and inelastic cross sections

Earlier calculations of rotationally inelastic cross sections in the low temperature range (10–50 K) for the $SO(^3\Sigma^-)$ collisions with He [22] indicated the presence of an F-conserving propensity rule, in keeping with what had been already found for O_2–He collisions [18] and with what had also been suggested to occur at ultralow energies for target molecules in their $^3\Sigma$ electronic states in general [8–13]. It is therefore of some interest to see how much of such conditions are preserved when going down to the Wigner regime of 10^{-6}–10^{-9} K for an ionic system.

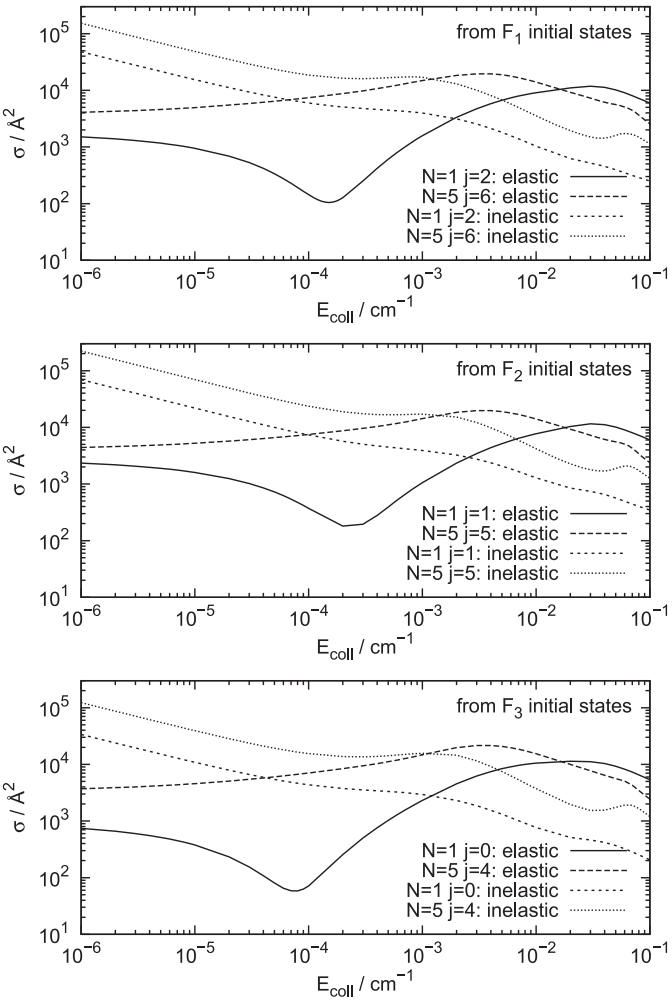

Fig. 3. Computed elastic and inelastic cross sections with initial states in the three possible F_i components. Top panel: $F_1 = |N, j = N + 1\rangle$; middle panel: $F_2 = |N, j = N\rangle$ and bottom panel: $F_3 = |N, j = N - 1\rangle$.

An interesting comparison among elastic and superelastic (cooling) cross sections is reported by the three panels of Figure 3.

The following features could be noted from a perusal of the data reported in that figure:

1. the inelastic cross sections, independently of the initial choice for the F_i state, become larger than the elastic cross sections very early on and remain substantially larger down to the Wigner regime ($<10^{-4}$ cm^{-1});
2. all the elastic processes which begin from the $N = 1$ rotational level show a marked minimum feature reminiscent of an effect like a Ramsauer-Townsend (RT) "dip" between 10^{-3} and 10^{-4} cm^{-1}, an indication of the presence of negative scattering lengths for the compound state resonances. As N increases, however, the effective potential gets modified and therefore this feature disappears. We have recently discussed similar behavior in ion-molecule relaxations at ultralow energies [26,27];

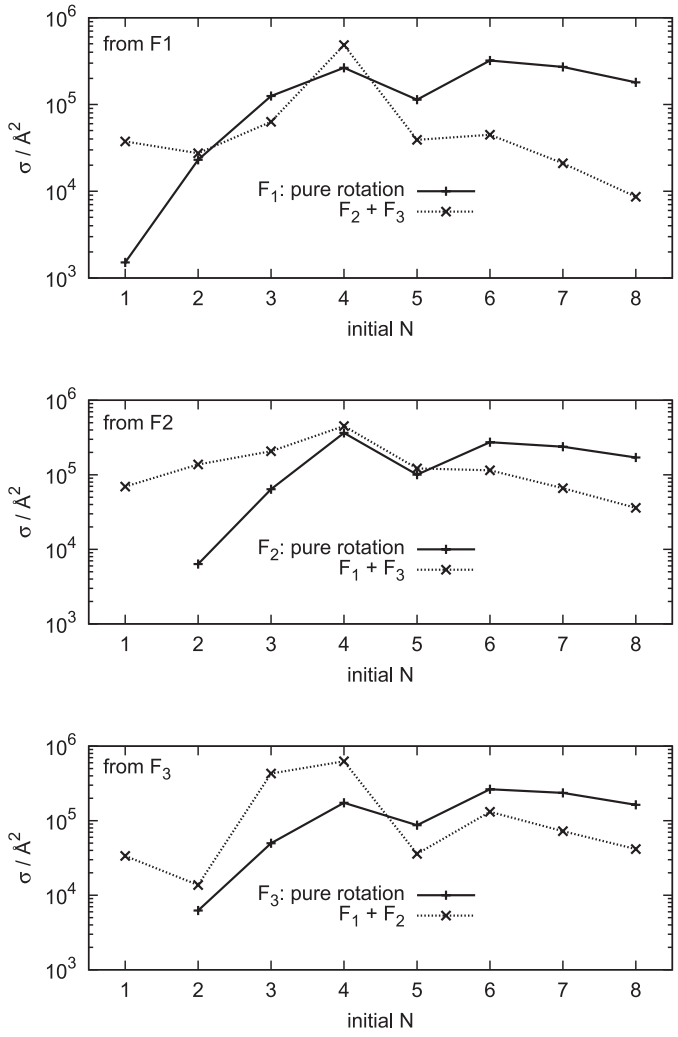

Fig. 4. Computed relaxation cross sections at 10^{-6} cm^{-1} of energy as a function of the initial rotational state N and for different initial F_i states, see main text for further details.

3. we report, as examples, two of the many computed relaxation cross sections we computed: we see in all three panels that total relaxation from higher N values (dotted curves) yield larger cross sections than when cooling occurs from lower-N states. This is to be expected since we are looking at larger sums over final states as N increases and it confirms also what found earlier on for other ionic systems [27].

One therefore can say that, even in the ultralow energy regimes, collisions involving ionic partners yield very efficient energy transfer processes and could rapidly produce rotationally colder molecular cations.

A different way of looking at the same set of processes is reported by Figure 4. We are showing in its three panels the cooling as a function of both the initial F_i state and the initial $|N\rangle$ rotational state. For each F_i state we also show the process which conserves the spin, and therefore conserves the F_i value (pure rotational relaxation), and those where both spin **and** rotational states change during the collision.

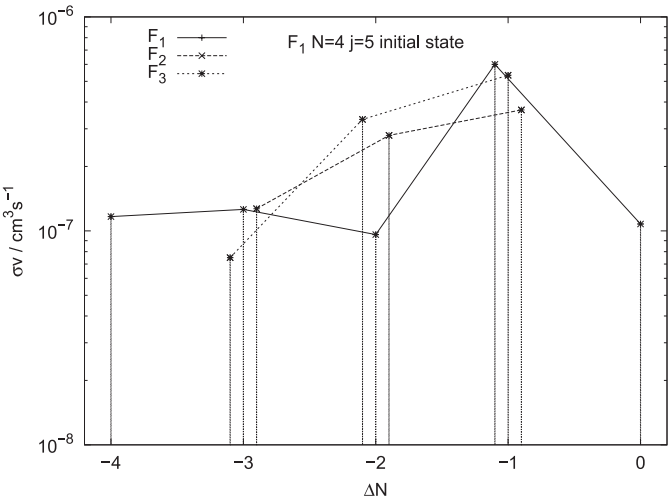

Fig. 5. Computed state-to-state rate values from the F_1 state, in the $|N = 4,\ j = 5\rangle$ initial target state, into all lower states. The data show σv, where v is the initial velocity.

In the case where the initial rotational state N is coupled with a spin state which is parallel to it (the F_1 spin-rotational state), we see that those transitions which conserve that orientation are increasingly associated with larger cross sections, especially for the larger N values: in other words, collisions which depolarize the spin state are depressed with respect to those which do not. We also see that, whenever the molecule is initially chosen to be in a high N state (i.e. up to $N = 8$), this behavior is true for all F_i choices and can be seen in all three panels.

On the other hand, when one starts from lower $|N\rangle$ states the "spin-flip" collisions are helpful in inducing overall relaxation: it really indicates a sort of energy-gap propensity since cross sections between lower-N values involve less energy transfer and produce larger cross sections in spite of the presence of spin-depolarization effects. In other words, the calculations of Figure 4 do indicate that F-conserving processes are yielding in general the larger cooling cross sections when the cation is occupying the higher $|N\rangle$ states; while they also suggest that the cooling from the lower rotational states does not reduce its efficiency when "spin-flip" processes are also occurring.

3.2 State-to-state cooling cross sections

A further analysis of the interplay between rotational cooling processes and spin-depolarizing collisions could be had by comparing individual cross sections, at the lowest considered collision energy of 10^{-6} cm^{-1}, as a function of various parameters which define the states involved in each process.

Figures 5 and 6 therefore report transitions from the initial F_1 state of two different rotational levels into all the lower $|N, j\rangle$ states available to such transitions and compare their relative sizes.

The transitions which do not involve any spin-polarization change by ending up into other F_1 states are

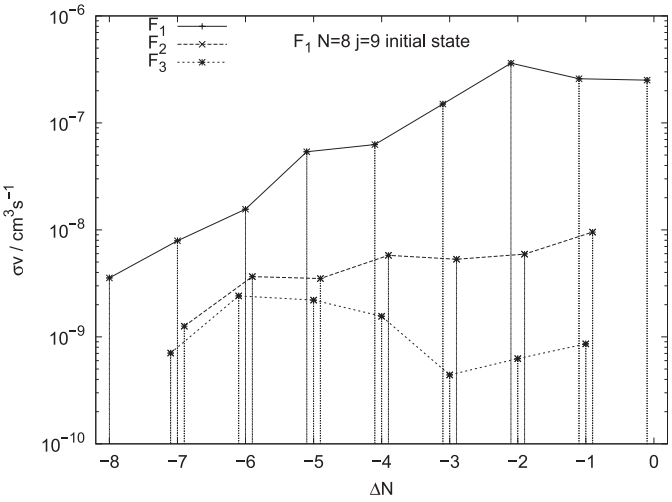

Fig. 6. Same as in Figure 5 but for the $|N = 8, j = 9\rangle$ initial target state. Collision energies at 10^{-6} cm^{-1}, as in Figure 5. The data show the state-to-state rate values as σv, v being the initial velocity at the chosen collision energy.

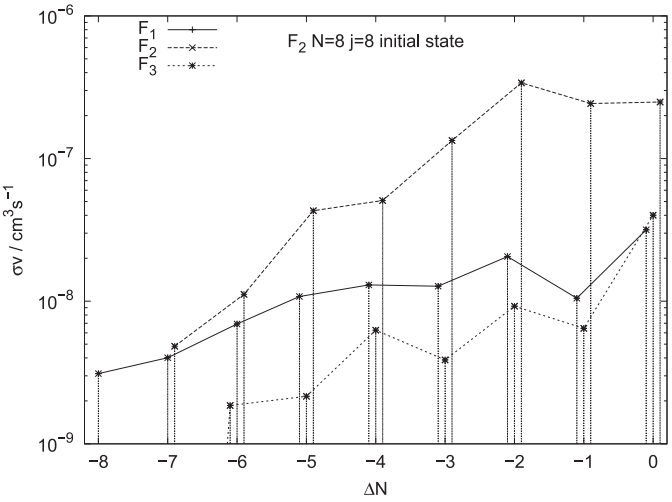

Fig. 7. Computed state-to-state relaxation rates (σv) at 10^{-6} cm^{-1} collision energy starting from the $|F_2\rangle$ configuration in the $|N = 8\rangle$ rotational level.

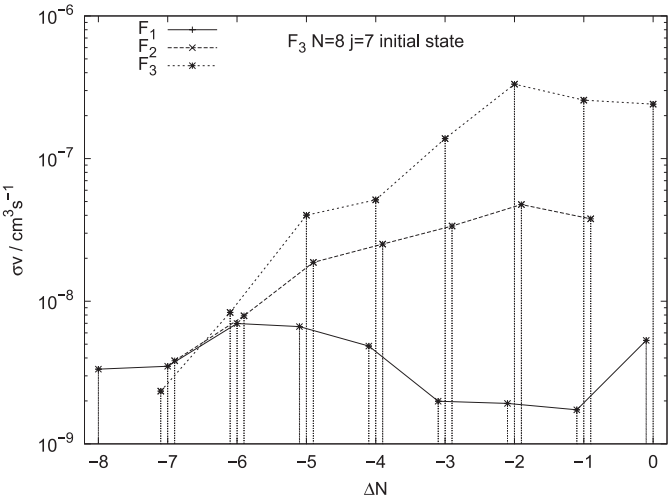

Fig. 8. Same as in Figure 7 but starting from the $|F_3\rangle$ configuration.

given by solid lines in both figures and we clearly see that, when $|N\rangle$ increases, to preserve spin polarization in the cationic target causes the rotational cooling probabilities to be much larger for all possible lower-N states. Even for the lowest initial N, however, we see that nearly all ΔN changes yield larger cross sections when the spin polarization is not changed. On the other hand, the rotational cooling process accompanied by spin-flip effects undergoes reduction of size nearly all the time, although such reduction is much more evident when the initial $|N\rangle$ state is high up on the rotational ladder.

The situation remains very similar even for the initial states $|F_2\rangle$ and $|F_3\rangle$, where the spin coupling with rotation is now less favorable. We show, in fact, the state-to-state cooling rates from the $|N = 8\rangle$ initial rotational level, for both types of initial configurations, in the data reported by Figures 7 and 8.

One clearly sees in Figure 7 that the spin-polarization preserving collisions (F-conserving) are the largest over the whole range of rotational relaxation processes, although summing over those processes where spin-flip occurs yields a larger value for each final N since those cross sections (for $F_2 \rightarrow F_1$ and $F_2 \rightarrow F_3$) are also fairly large.

The results for the transitions from the F_3 configuration $|N, N-1\rangle$ are slightly less obvious, but they also indicate in Figure 8 that the spin-conserving processes yield larger cross sections for nearly all the ΔN processes listed there. In other words, we see that (i) all state-to-state relaxation cross sections become very large at ultralow energies, as expected for this ionic system with a stronger interaction than the neutral cases [12,13], and (ii) that they also show their largest size when spin-polarization changes do not occur during the relaxation process. Hence, it is fair to conclude from our calculations that the rotational relaxation of an open-shell electronic state of an ionic target by ultralow energy collision is an efficient process, one which is helped when occurring without concurrent spin-depolarization effects.

3.3 Relaxation rates at the Wigner's regime

In order to examine more globally the findings from the broad range of state-to-state cross sections which we have computed in the present study, we have also calculated the global rates as a function of the initial j state ($j = N + S$) by exploiting the relation [28]

$$\Gamma_j(T \rightarrow 0) = \frac{4\pi\beta_j\hbar}{\mu} \tag{12}$$

where β_j is the imaginary part of the scattering length which can be obtained from the total quenching cross

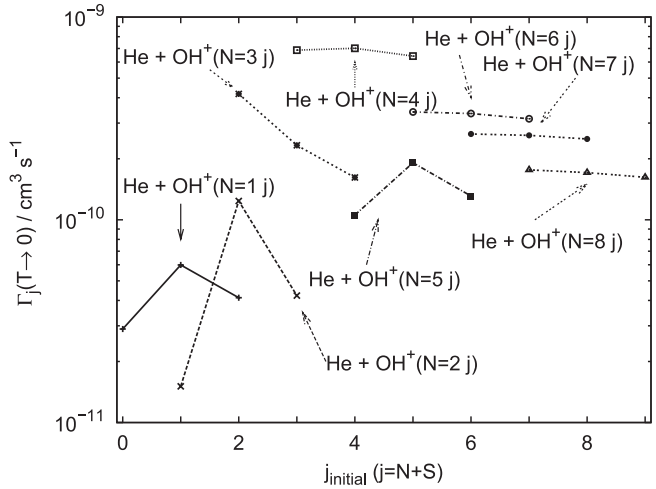

Fig. 9. Computed rates from different $|N, j\rangle$ initial states of the cationic target. In each of the triads, the F-conserving rate corresponds to the central point.

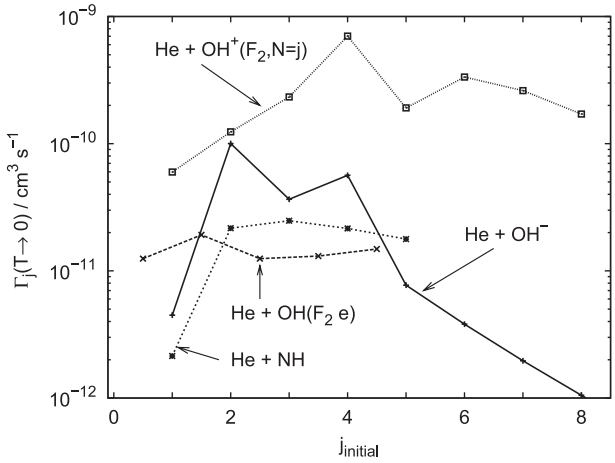

Fig. 10. Computed relaxation rates at vanishing temperature for several polar hydrides. see main text for details.

section, σ_j^{in}, in the limit of vanishing kinetic energy [29]

$$\beta_j = \lim_{k_j \to 0} \frac{k_j \sigma_j^{in}}{4\pi}. \tag{13}$$

The results for the rates obtained with the present system are reported by Figure 9 and we show for each rate the F-conserving values (central point), together with the two spin-flip cases.

By comparing the rates from the lowest possible rotational state ($N = 1$) with those from the highest rotational level we have considered ($N = 8$), we clearly see that the latter are nearly one order of magnitude larger than the former. we also see that the F-conserving rates (center points in each triads) are invariably the larger ones, this being more so when one starts from the lower-N state. The case of $N = 4$ is showing the largest rates of all, indicating a sort of "magic number" along the lower echelons of the rotational ladder in $OH^+(^3\Sigma^-)$: rates from larger N values become, in fact, smaller in size as N increases.

To better place the present findings with respect to the behavior of other similar systems, we compare limiting relaxation rates in Figure 10 with those of diatomic molecules also cooled by buffer He gas loading.

The figure reports the earlier calculations for the global rotational cooling rates, from various initial rotational levels, for the NH–He system [30], the relaxation for the OH–He system [31] and our earlier results for the OH^-–He dynamics [25]. The present findings on the OH^+–He system are shown for the cooling rates of the $|F_2\rangle$ configuration from various initial rotational levels.

It is interesting to note the following features exhibited by the systems examined

1. all cooling rates are seen to depend on the initial rotational level selected for relaxation, although the rates are not increasing in any simple fashion as $|j\rangle$ increases as shown by nonpolar, neutral systems under similar conditions [32]. However, different systems show different specific states to be "magic" in the sense that their cooling rates are larger than those of their neighboring levels;
2. the cationic hydride exhibits the strongest form of interaction with the buffer gas and therefore we find that its collisional relaxations show the largest values with respect to those of similar systems which carry no charge;
3. the variation of cooling efficiency in going from neutral OH to the positive ion OH^+ is therefore seem to span between one and two orders of magnitudes and to definitely suggest its cooling process to be the most efficient with respect to other polar hydrides using He as a buffer gas.

4 Present conclusions

In this work we have analysed the collisional efficiency of rotational cooling of $OH^+(^3\Sigma^-)$ under buffer gas loading conditions at ultralow energies and considering ^{4}He as a possible partner.

The exact quantum calculations have employed a fairly accurate, ab initio potential energy surface computed earlier in our laboratory which describes the spatial coupling via the anisotropy of the interaction between the ^{4}He projectile and the spin-rotational description of the target molecule. The quantum calculations indicate that collisional inelastic processes to be efficient for the title system and that their corresponding cross sections become larger than the purely elastic ones around 10^{-3} cm^{-1} of collision energy. Furthermore, our computations found that those transitions which conserve the spin alignment (F-conserving transitions) produce the larger cross sections, this being even more so when the cooling processes occur from the higher-N as initial states of the target.

An analysis of the behavior of the state-to-state relaxation cross sections further revealed that the occurrence of "spin-flip", or spin depolarization, during collisions depresses the corresponding rotational inelasticity that occurs in conjunction with the former process, while the pure

rotational cooling without loss of spin orientation invariably yields larger relaxation cross sections.

The cumulative relaxation rates as a function of the initial rotational state, or of the initial spin-rotation state, confirm the above findings and also indicate that the cationic hydride is very efficiently cooled by collision with ^{4}He, certainly more efficiently that its neutral counterpart or its isoelectronic, neutral NH molecule, as shown by our present comparison.

The financial supports of the Research Committee of the University of Rome "La Sapienza", of the CASPUR Supercomputing Center, of the EU Network "Comol" HPRN-CT-2002-00290 and of the National Research Project PRIN 2004, are gratefully acknowledged. We are also grateful to professor John Brown for his generous help and advice in the choice of the OH^+ rotational parameters employed in our work.

References

1. E.g. see I.S. Vogelius, L.B. Madsen, M. Drewsen, Phys. Rev. A **70**, 053412 (2004)
2. I.S. Vogelius, L.B. Madsen, M. Drewsen, Phys. Rev. Lett. **89**, 173003 (2002)
3. E.g. see E. Herbst, S. Knudson, Astrophys. J. **245**, 529 (1981)
4. J. Mikosch, H. Kreckel, R. Wester, R. Plasil, J. Glosik, D. Gerlich, D. Schwalm, A. Wolf, J. Chem. Phys. **121**, 11030 (2004)
5. D.J. Larson, J.C. Bergquist, J.J. Bollinger, W.M. Itano, D.J. Wineland, Phys. Rev. Lett. **57**, 70 (1986)
6. P. Bowe, L. Hornekaer, C. Brodersen, M. Drewsen, J.S. Hangst, J.P. Schiffer, Phys. Rev. Lett. **82**, 2071 (1999)
7. B. Roth, P. Blythe, H. Daerr, L. Paracchini, S. Schiller, J. Phys. B **39**, S1241 (2006)
8. J.L. Bohn, Phys. Rev. A **62**, 032701 (2000)
9. J.L. Bohn, Phys. Rev. A **63**, 052714 (2001)
10. T.V. Tscherbul, R. Krems, J. Chem. Phys. **125**, 194311 (2006)
11. T.V. Tscherbul, R. Krems, Phys. Rev. Lett. **97**, 083201 (2006)
12. R. Krems, A. Dalgarno, J. Chem. Phys. **120**, 2296 (2004)
13. R. Krems, Int. Rev. Phys. Chem. **24**, 99 (2005)
14. F. Marinetti, E. Bodo, F.A. Gianturco, J. Comp. Theor. Chem. **5**, 543 (2006)
15. S.F. Boys, F. Bernardi, Mol. Phys. **19**, 553 (1970)
16. E. Bodo, F.A. Gianturco, E. Yurtsever, J. Low Temp. Phys. **138**, 259 (2005)
17. J.M. Brown, J.T. Hougen, K.P. Huber, J.W.C. Johns, I. Kopp, H. Levebvre-Brion, A.J. Meter, D.A. Ramsay, J. Rostas, R.N. Zare, J. Mol. Spectrosc. **55**, 500 (1975)
18. G.C. Corey, M.H. Alexander, J. Schaefer, J. Chem. Phys. **85**, 2726 (1986)
19. J.T. Hougen, Natl. Bur. Stand. (US) Monogr. **115**, 109 (1970)
20. J.M. Brown, private communucation (2006)
21. M.H. Alexander, P.J. Dagdigian, J. Chem. Phys. **79**, 302 (1983)
22. F. Lique, A. Spielfield, M.-L. Dubernet, N. Feautier, J. Chem. Phys. **123**, 134316 (2005)
23. G.C. Corey, F.R. McCourt, J. Phys. Chem. **87**, 2723 (1983)
24. R. Martinazzo, E. Bodo, F.A. Gianturco, Comp. Phys. Comm. **151**, 187 (2003)
25. L. Gonzalez-Sanchez, F. Marinetti, E. Bodo, F.A. Gianturco, J. Phys. B **39**, 1203(2006)
26. E. Bodo, E. Scifoni, F. Sebastianelli, F.A. Gianturco, A. Dalgarno, Phys. Rev. Lett. **89**, 283201 (2002)
27. E. Bodo, F.A. Gianturco, Europhys. Lett. **77**, 3301 (2007)
28. N. Balakrishnan, V. Kharchenko, R.C. Forrey, A. Dalgarno, Chem. Phys. Lett. **280**, 5 (1997)
29. E.P. Wigner, Phys. Rev. **73**, 1002 (1948)
30. R.V. Krems, H.R. Sadeghpour, A. Dalgarno, D. Zgid, J. Klos, G. Chalasinski, Phys. Rev. A **68**, 051401(R) (2003)
31. L. Gonzalez-Sanchez, E. Bodo, F.A. Gianturco, Phys. Rev. A **73**, 022703 (2006)
32. E. Bodo, F.A. Gianturco, F. Sebastianelli, E. Yurtsever, M. Yurtsever, Theor. Chem. Acc. **112**, 263 (2004)